In Vivo Mitochondrial Oxygen Tension Measured by a Delayed Fluorescence Lifetime Technique

Egbert G. Mik,*† Tanja Johannes,*‡ Coert J. Zuurbier,§ Andre Heinen,§ Judith H. P. M. Houben-Weerts,¶ Gianmarco M. Balestra,* Jan Stap,‖ Johan F. Beek,** and Can Ince*

*Department of Physiology, Academic Medical Center, University of Amsterdam, Amsterdam, The Netherlands; †Department of Anesthesiology, Erasmus Medical Center, University of Rotterdam, Rotterdam, The Netherlands; ‡Department of Anesthesiology and Critical Care, University Hospital Tuebingen, Tuebingen, Germany; and §Department of Anesthesiology, ¶Department of Medical Biochemistry, ‖Center for Microscopical Research, Department of Cell Biology and Histology, and **Laser Center, Academic Medical Center, University of Amsterdam, Amsterdam, The Netherlands

ABSTRACT Mitochondrial oxygen tension ($mitoPO_2$) is a key parameter for cellular function, which is considered to be affected under various pathophysiological circumstances. Although many techniques for assessing in vivo oxygenation are available, no technique for measuring $mitoPO_2$ in vivo exists. Here we report in vivo measurement of $mitoPO_2$ and the recovery of $mitoPO_2$ histograms in rat liver by a novel optical technique under normal and pathological circumstances. The technique is based on oxygen-dependent quenching of the delayed fluorescence lifetime of protoporphyrin IX. Application of 5-aminolevulinic acid enhanced mitochondrial protoporphyrin IX levels and induced oxygen-dependent delayed fluorescence in various tissues, without affecting mitochondrial respiration. Using fluorescence microscopy, we demonstrate in isolated hepatocytes that the signal is of mitochondrial origin. The delayed fluorescence lifetime was calibrated in isolated hepatocytes and isolated perfused livers. Ultimately, the technique was applied to measure $mitoPO_2$ in rat liver in vivo. The results demonstrate $mitoPO_2$ values of ~30–40 mmHg. $mitoPO_2$ was highly sensitive to small changes in inspired oxygen concentration around atmospheric oxygen level. Ischemia-reperfusion interventions showed altered $mitoPO_2$ distribution, which flattened overall compared to baseline conditions. The reported technology is scalable from microscopic to macroscopic applications, and its reliance on an endogenous compound greatly enhances its potential field of applications.

INTRODUCTION

Mitochondrial oxygen tension ($mitoPO_2$) is a key parameter for cellular function. This is not only because oxygen is indispensable as an oxidant in the mitochondrial respiratory chain (1). Mitochondria are also thought to play a major role in cellular oxygen sensing (2,3) and oxygen-regulated gene expression (4). Because of its importance, many techniques have been developed to measure oxygen tension in vivo (5). The available techniques are, however, limited in several respects: either they are locally destructive, such as the use of oxygen electrodes (6), or they rely on the injection of a foreign compound, such as in phosphorescence quenching (7,8) and electron paramagnetic resonance oximetry (9). Although these techniques make it possible to directly measure interstitial or microvascular PO_2, they provide only an indirect estimate of $mitoPO_2$. Thus there is a real need for in vivo techniques that can quantitatively and noninvasively measure $mitoPO_2$ to elucidate cellular oxygenation under various pathophysiological circumstances.

Recently we reported that the delayed fluorescence lifetime of endogenous protoporphyrin IX (PpIX) can be used to measure $mitoPO_2$ in cultured cells (10). Such an approach might also work in vivo and provide a breakthrough technique with a real potential for clinical application. A major advantage of such a technique would be that the basic setup for delayed fluorescence lifetime measurements is relatively simple and straightforward. Furthermore, since the technique relies on the optical properties of an endogenously synthesized compound, it potentially has a wide field of applications. Being an optical technique, it would be downscalable from macroscopic to microscopic measurements, even further increasing its versatility. Since delayed fluorescence has much in common with phosphorescence, it shares the useful ability to recover oxygen histograms from a volume of tissue with high temporal resolution (11,12). For in vivo measurements, another crucial factor is that lifetime measurements are not disturbed by changes in tissue optical properties (such as scatter and absorption) as can occur with, e.g., changes in hemoglobin content or saturation. This allows true quantitative measurements to be made instead of relative or semi-quantitative measurements.

Accordingly, we have developed a novel in vivo delayed fluorescence lifetime technique that quantitatively measures $mitoPO_2$ using the oxygen-dependent optical properties of endogenously synthesized PpIX. In this article, we describe the development and applicability of this technique for direct measurements of $mitoPO_2$ in the intact organism. We report that delayed fluorescence can be obtained from various tissues in the rat, and demonstrate that the signal is of mitochondrial origin and can be calibrated in rat liver. Ultimately, we provide the first direct measurements of both global and

Submitted November 19, 2007, and accepted for publication June 24, 2008.

Address reprint requests to Egbert G. Mik, MD, Dept. of Anesthesiology, Erasmus Medical Center, Rotterdam s-Gravendijkwal 230, 3015 CE Rotterdam, The Netherlands. Tel.: 31-6-47890339; Fax: 31-10-7033722; E-mail: e.mik@erasmusmc.nl.

Editor: Michael Edidin.

0006-3495/08/10/3977/14 $2.00

doi: 10.1529/biophysj.107.126094

regional mitoPO$_2$ within the liver in vivo in healthy and pathological conditions.

MATERIALS AND METHODS

The concept: from PpIX accumulation to mitoPO$_2$ histogram

PpIX is the final precursor of heme in the heme biosynthetic pathway. PpIX is synthesized in the mitochondria (13), and administration of its precursor 5-aminolevulinic acid (ALA) to cells and organisms substantially enhances PpIX concentration (14). Since the conversion of PpIX to heme is a rate-limiting step, administration of ALA causes accumulation of PpIX in the mitochondria (10) (Fig. 1 *a*). PpIX possesses a triplet state (T_1) that reacts strongly with oxygen (15), making the T_1 lifetime oxygen-dependent (Fig. 1 *b*). Population of T_1 occurs upon excitation with a pulse of blue or green light, and bidirectional intersystem crossing causes the emission of red delayed fluorescence (10). The lifetime of the delayed fluorescence reflects the T_1 lifetime and can therefore be used to measure oxygen (Fig. 1 *c*).

The basic setup for delayed fluorescence lifetime measurements in the in vivo condition consists of an excitation source, an optical flexible fiber to excite the organ/tissue of choice, a detector, a means to discriminate emission from excitation and background light, and a data-acquisition system with subsequent signal processing and analysis. A block diagram of the time-domain device used in this study is shown in Fig. 1 *d*. In the case of heterogeneity in mitoPO$_2$, as is expected to occur in intact tissue, locations with different mitoPO$_2$ emit delayed fluorescence with different lifetimes. Therefore, the observed overall delayed fluorescence signal does not decay monoexponentially, but contains a lifetime distribution (Fig. 1 *e*). This allows mathematical recovery of the underlying mitoPO$_2$ distribution, providing detailed insight into the heterogeneity. Details of the setup and the lifetime deconvolution algorithm are provided below.

Delayed fluorescence setup

The setup was an adapted version of the previously described delayed fluorescence system (10). The pulsed laser system consisted of a Quanta-Ray DCR-3D (Spectra-Physics, Mountain View, CA) pumping a tunable optical parametric oscillator OPO-A355 (GWU Lasertechnik Vertriebs GmbH, Erftstadt-Friesheim, Germany) containing a β-barium-borate crystal and providing pulses of 2–4 ns (510 nm, 0.2 mJ/pulse output at fiber ending). The laser light was directed to the tissue by a multimode fiber with core diameter of 400 μm. The detector was a gated R928 red-sensitive photomultiplier tube (Hamamatsu, Hamamatsu City, Japan) combined with a monochromator (model 77320; Oriel Corp., Stratford, CT) set at a wavelength of 635 nm. Signal processing was performed by an in-house-built integrator with an integration time of 3.5 μs and a reset time of 0.5 μs. A PC-based data-acquisition system using a PCI-MIO-16E1 data acquisition board (National Instruments, Austin, TX) sampled the signal at 250 kHz and averaged 64 laser pulses (repetition rate 20 Hz) before analysis. Control of the setup and analysis of the data were performed with software written in LabView (National Instruments, Austin, TX).

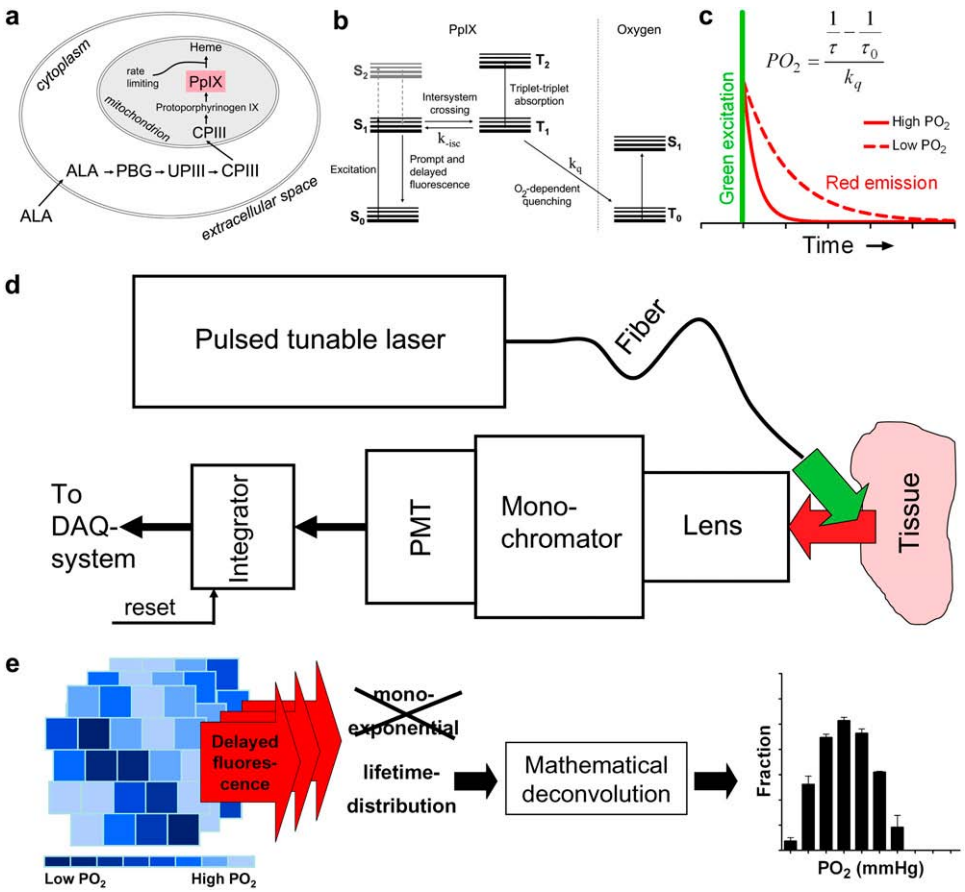

FIGURE 1 Principle of mitoPO$_2$ measurement by oxygen-dependent quenching of ALA enhanced PpIX. (*a*) Principle by which ALA administration enhances mitochondrial PpIX levels. ALA, 5-aminolevulinic acid; PBG, porphobilinogen; UPIII, uroporphyrinogen III; CPIII, coporporphyrinogen III; and PpIX, protoporphyrin IX. (*b*) Jablonski diagram of states and state transitions of PpIX and its interaction with oxygen. S_0, S_1, and S_2 represent the ground state and first and second excited singlet states, respectively. T_0, T_1, and T_2 represent the ground (triplet) state and first and second excited triplet states, respectively. k_q is the rate constant of T_1 quenching by oxygen. (*c*) PpIX emits delayed fluorescence after excitation by a pulse of green (510 nm) light. The delayed fluorescence lifetime is oxygen-dependent according to the Stern-Volmer equation (inset), in which k_q is the quenching constant and τ_0 is the lifetime at zero oxygen. (*d*) Example of the delayed fluorescence setup. PMT denotes photomultiplier, and DAQ denotes data acquisition. Details are provided in the Materials and Methods section. (*e*) Tissue comprised of regions with different mitoPO$_2$s, each with a different delayed fluorescence lifetime. The overall signal therefore contains a lifetime distribution that can be mathematically converted into a mitoPO$_2$ histogram.

Recovery of mitoPO_2 histograms

In the case of a nonhomogeneous mitoPO_2, the delayed fluorescence signal generally can be described by an integral over an exponential kernel:

$$y(t) = \int_0^t \exp(-\lambda t) f(\lambda),$$

where $f(\lambda)$ denotes the spectrum of reciprocal lifetimes that should be determined from the finite data set $y(t)$. According to Golub et al. (11), a detailed recovery of the underlying oxygen distribution can be obtained by assuming that the delayed fluorescence signal can be described by a sum of rectangular distributions with an adequately small chosen width (2δ), resulting in the following fit equation:

$$Y^*(t) = Y(t)[\exp(k_0 t)k_q \delta t/\sinh(k_q \delta t)] = \sum w_i \exp(-k_q Q_i t),$$

where $Y(t)$ is the normalized delayed fluorescence data, k_0 is the first-order rate constant for delayed fluorescence decay in the absence of oxygen, k_q is the quenching constant, and w_i is the weight factor for the according bin with central PO_2 Q_i and width 2δ ($w_i \geq 0$ and $\sum w_i = 1$). Recently, this approach was successfully used by our group for the recovery of microvascular PO_2 histograms from phosphorescence lifetime measurements (12).

For our analysis we chose δ to be 5 mmHg since this allows detailed resolution of PO_2 histograms while keeping the transformation factor for $Y^*(t)$ below 1, diminishing the influence of noise in the tail of the delayed fluorescence signal (11). Using a 10-bin histogram, this allows the recovery of oxygen histograms over the physiological range of 0–100 mmHg. Recovery of oxygen histograms from the photometric signal was performed with the GraphPad Prism package (Version 4, GraphPad Software, San Diego, CA) using the Marquart-Levenberg nonlinear fit procedure.

Animals

The protocol was approved by the Animal Research Committee of the Academic Medical Center at the University of Amsterdam. Animal care and handling were performed in accordance with the guidelines for Institutional and Animal Care and Use Committees.

Animal preparation

A total of 26 male Wistar rats (Charles River, Wilmington, MA), with body weights between 300 and 400 g, were anesthetized by an intraperitoneal injection of a mixture of ketamine 90 mg kg^{-1}, medetomidine 0.5 mg kg^{-1}, and atropine 0.05 mg kg^{-1}. Ketamine 50 mg kg^{-1} h^{-1} was infused intravenously to maintain anesthesia. Mechanical ventilation was performed via tracheotomy. Ventilation was adjusted on end-tidal PCO_2, keeping the arterial PCO_2 between 35 and 40 mmHg. Variations in FiO_2 were made by mixtures of oxygen and nitrogen. Unless stated otherwise, FiO_2 was set at 40%. For intravenous administration of drugs and fluids (NaCl as solvent for ALA, and Ringer's lactate for maintenance), a polyethylene catheter (outer diameter = 0.9 mm) was inserted into the right jugular vein. Arterial blood pressure and heart rate were monitored with a similar catheter in the right carotid artery. Crystalloid solution 5 mL kg^{-1} h^{-1} was administered continuously. Body temperature was rectally measured and kept at 37°C ± 0.5°C by means of a heating pad.

The liver was exposed by midline laparotomy. Ischemia-reperfusion was performed by a method inducing partial hepatic ischemia (70%) as described elsewhere (16). In short, after dissection of the falciform ligament, the afferent vessels to the median and left lateral lobes were exposed by inverting the hepatic lobes upward. An atraumatic vascular clip was applied to these vessels to induce partial hepatic ischemia. In this way, cessation of the blood flow to the clipped lobes was complete, but the remaining perfused lobes prevented mesenteric congestion by allowing drainage of the portal vein. Delayed fluorescence signals during ischemia-reperfusion were obtained from the nonperfused lobes.

In a separate group of animals ($n = 5$), ALA was administered 2 h before the experiment by injection into the tail vein during pentobarbital anesthesia (60 mg/kg). After the ALA injection, the rats were allowed to recover for 2 h in the cage before being anesthetized with ketamine, medetomedine, and atropine as described above. Mechanical ventilation was performed via tracheotomy, and anesthesia was maintained with ketamine. Ventilation was adjusted on end-tidal PCO_2 as described above and the liver was exposed by midline laparotomy. In these rats we performed experiments in which the oxygen concentration of the ambient atmosphere at the surface of the liver was altered using a previously described gas flow system (17). This system allowed application of gas mixtures (N_2/O_2) with varying oxygen concentrations to the organ surface at a rate of 250 mL/min. The gas was humidified and prewarmed so that it would not cool down or dry out the surface of the liver. Furthermore, the abdomen was loosely covered with Saran Wrap to shield the liver from convective air. The actual oxygen concentration at the surface (the site of measurement) was measured using a needle-type fiber-optic microsensor (OxyMicro System, World Precision Instruments, Sarasota, FL).

Isolated hepatocytes

Rat liver parenchymal cells were isolated according to a classic method (18). Cells were stored in Krebs-Henseleit solution and continuously gassed with 95% oxygen and 5% carbon dioxide until used for analysis. Calibration experiments were performed using a rotational cell oxygenator as described elsewhere (10). Oxygen consumption was blocked by a mixture of 2 mM sodium cyanide, 1 μM rotenone, and 10 μM diphenyleneiodonium chloride (all chemicals from Sigma, St. Louis, MO).

Isolated liver

After isolation the livers were retrograde-perfused via the vena porta with Krebs-Henseleit buffer at a continuous flow (35 mL/min). The oxygen content of the buffer was adjusted while keeping the carbon dioxide at 5% as previously described (17). Inhibition of cellular respiration was performed as described for isolated hepatocytes.

Isolated mitochondria

Mitochondria were isolated from the livers of animals treated with ALA (200 mg/kg) dissolved in 0.9% NaCl ($n = 4$) or with normal saline only ($n = 4$), 2–3 h before isolation. The isolation procedures were performed as reported previously (19). In short, the livers were placed in isolation buffer (200 mM mannitol, 50 mM sucrose, 5 mM KH_2PO_4, 5 mM MOPS, 1 mM EGTA, and 0.1% bovine serum albumin), minced into small pieces, and homogenized. The homogenate was centrifuged at 3220 *g* for 10 min. The pellet was resuspended in isolation buffer and centrifuged at 800 *g* for 10 min, and the remaining supernatant was centrifuged at 3220 *g* for 10 min. The final pellet was resuspended in isolation buffer and kept on ice, and the protein content was determined by the Bradford method. All procedures were performed at 4°C. Mitochondrial oxygen consumption was measured polarographically at 37°C in a respirometer, using mitochondria (1.0 mg protein/mL) resuspended in respiration buffer. Respiration was initiated with 10 mM succinate + 10 μM rotenone (state 2 respiration), followed by addition of 400 μM ADP (state 3 respiration). The respiratory control index (RCI) was calculated as the state 3 to state 4 ratio. All chemicals were obtained from Sigma (St. Louis, MO).

Fluorescence microscopy

Fluorescence microscopy was performed using a Leica fluorescence microscope (DM RA HC, Leica Microsystems GmbH, Wetzlar, Germany) with a cooled charge-coupled device camera (KX1400, Apogee Instruments, Roseville, CA) and CY3 band-pass filter set. We observed freshly isolated hepatocytes and used the rapid photobleaching of PpIX as the contrast-enhancing technique (10).

Simulation of the photometric signal

LabView (Version 7.1, National Instruments, Austin, TX) was used for simulation of delayed fluorescence emission in heterogeneous systems. Oxygen distributions were generated by a Monte Carlo approach for Gaussian distributions. Either a single Gaussian distribution or, to simulate more complex distributions, a combination of two Gaussian distributions was used to simulate an overall oxygen distribution. The mean and standard deviation (SD) of the individual Gaussian distributions, as well as relative contribution of the two Gaussian distributions to the overall oxygen distribution, could be freely chosen. The eventual oxygen distributions consisted of 200 equally wide bins over a range of 0–200 mmHg. The simulated oxygen distributions were used to generate a simulated photometric signal. To this end, a sum of 200 exponentials was generated with weight factors determined by the oxygen distribution, and lifetimes dictated by the quenching constants of protoporphyrin IX. The resulting trace was normalized and noise was added with varying signal/noise ratio (SNR). Here, SNR is defined as the ratio of maximum signal amplitude to the peak-to-peak noise (noise for a single simulated event is equal to the total amplitude of noise times a random number on the symmetrical interval [−0.5, 0.5]).

Statistical analysis

Data are expressed as the mean ± SD.

RESULTS

ALA administration induced delayed fluorescence in vivo

To enhance tissue PpIX levels in vivo, ALA (Sigma, St. Louis, MO; 200 mg/kg in 10 min) was administered intravenously via a jugular vein catheter to anesthetized and mechanically ventilated rats. Two hours after ALA administration, delayed fluorescence was observed in various tissues. To test the oxygen dependency of the delayed fluorescence lifetime, interventions that either globally (changes in the fraction of inspired oxygen (FiO_2)) or locally (cessation of blood flow) altered oxygen delivery to the tissue were undertaken. Lowering of the FiO_2 resulted invariably in a prolonging of the delayed fluorescence lifetime, e.g., in rectus abdominis muscle (Fig. 2 *a*). In the skin of the back paw, cessation of blood flow by ligation of the limb also resulted in prolonging of the lifetime (Fig. 2 *b*) in accordance with a reduction in PO_2. ALA administration induced oxygen-dependent delayed fluorescence in all observed tissues,

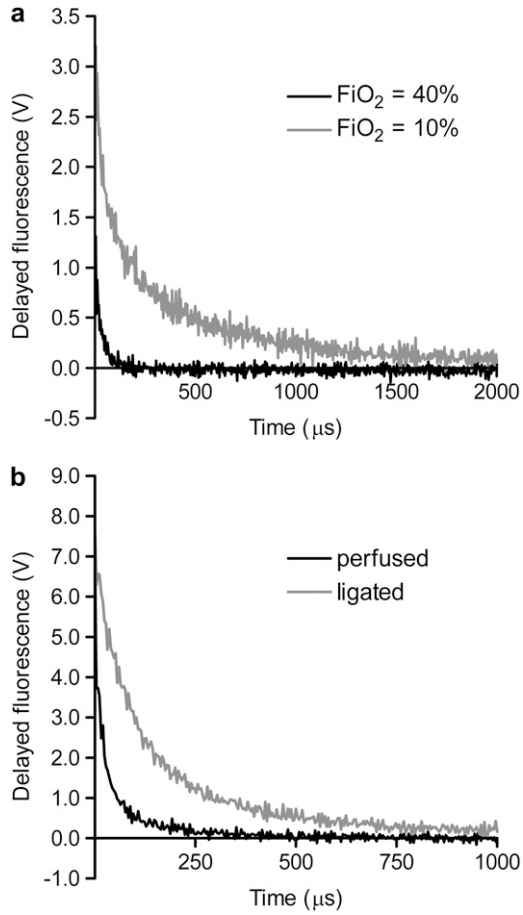

FIGURE 2 Intravenous ALA administration induces oxygen-dependent delayed fluorescence in tissues. (*a*) Delayed fluorescence signals from rat abdominal muscle at different FiO_2 concentrations. (*b*) Delayed fluorescence signals from the skin of a rat paw before and 2 min after cessation (tourniquet) of blood supply to the limb.

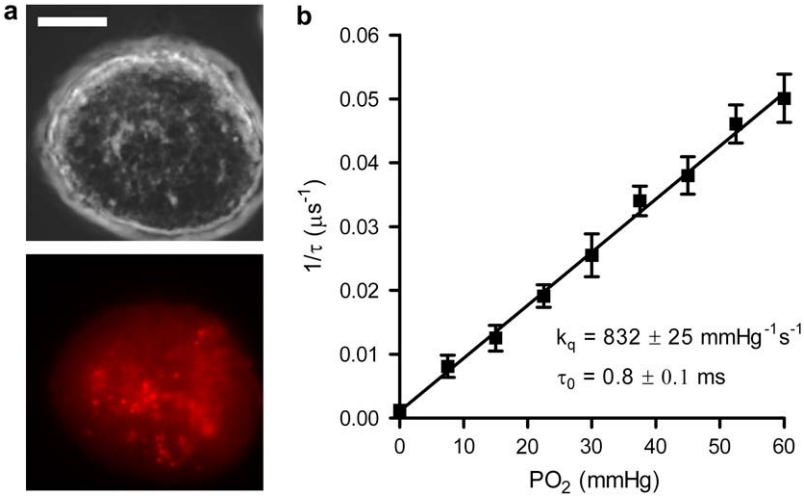

FIGURE 3 PpIX is induced in the mitochondria by intravenous ALA administration, and its delayed fluorescence lifetime can be used to measure mitochondrial PO_2. (*a*) Microscopic image of a single isolated hepatocyte, phase contrast (upper panel) and PpIX fluorescence (lower panel). The scale bar denotes 10 μm. The patchy pattern is typical for mitochondrial localization (10). (*b*) Reciprocal delayed fluorescence lifetime ($1/\tau$) versus PO_2 in suspensions of isolated hepatocytes. Inserted is the Stern-Volmer equation in which k_q is the quenching constant and τ_0 is the lifetime at zero oxygen. The error bars indicate the SD ($n = 6$).

including gut, kidney, liver, heart, lung, skin, and muscle. No delayed fluorescence was observed in blood.

Calibration of the PpIX signal in isolated hepatocytes

To establish the mitochondrial localization of the ALA-induced PpIX and the usability of the delayed fluorescence lifetime for quantitative PO_2 measurements, we further focused our experiments on the liver. This is because the liver provides all the components needed for our proof of principle: a high signal level, a standard technique for isolation of hepatocytes, and the possibility of obtaining measurements in an isolated perfused organ.

The mitochondrial origin of the delayed fluorescence signal was confirmed by fluorescence microscopy on isolated hepatocytes (Fig. 3 *a*). PpIX fluorescence had an intracellular origin and showed an inhomogeneous spot-like appearance (Fig. 3 *a*), as found in other cell types for which colocalization of the PpIX and mitochondria has been demonstrated (10).

Delayed fluorescence was measured in suspensions of freshly isolated hepatocytes subjected to various levels of oxygen. The calibration experiments showed excellent correlation between reciprocal lifetime and PO_2 (Fig. 1 *b*), as described by the Stern-Volmer relation. The calibration constants were $k_q = 832$ mmHg^{-1}s^{-1} and $\tau_0 = 0.8$ ms, and were similar to previously reported values in cultured cell types (10).

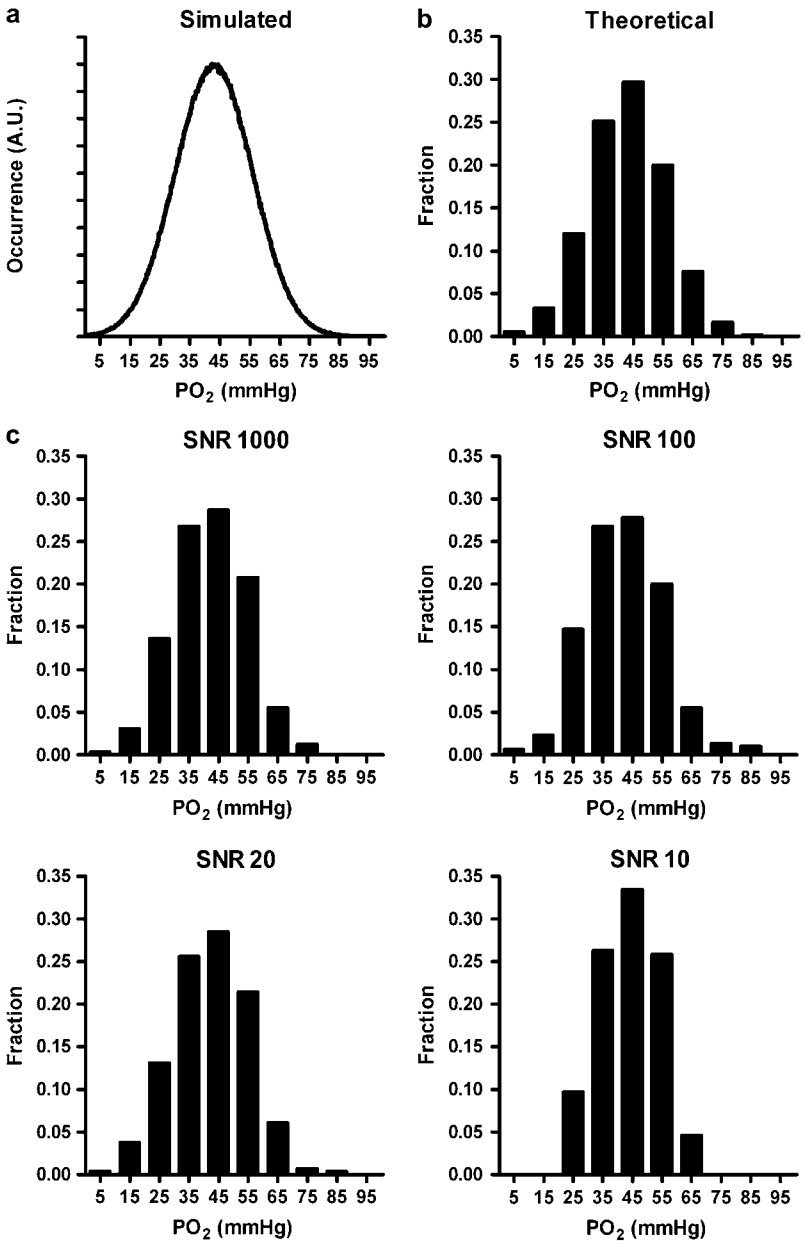

FIGURE 4 Effect of altered SNR on the ability of the histogram fitting procedure to recover the original computer-generated Gaussian distribution of PO_2. (*a*) The simulated Gaussian oxygen distribution (mean = 43 mmHg; SD = 13 mmHg). (*b*) The theoretical oxygen histogram (result from dividing the oxygen distribution into 10 bins). (*c*) Effect of decreasing SNR on the shape of recovered oxygen histograms.

Performance of the deconvolution method

For the recovery of oxygen distributions from the delayed fluorescence signals, we used an existing deconvolution method that was introduced by Golub et al. (11). In their original article, Golub et al. extensively described the background of the method and analyzed its performance in application to phosphorescence lifetime measurements with the oxygen-sensitive dye Pd-meso-tetra (4-carboxyphenyl) porphine. Their analysis showed that the method was able to provide accurate recovery of oxygen distributions and, moreover, had the very favorable property of being relatively insensitive to noise. However, the performance of the deconvolution algorithm is dependent on the quenching constants and lifetime range. Therefore, based on the original approach of Golub et al., we extensively tested the method for the quenching constants of protoporphyrin IX by using computer simulations.

To test the sensitivity of the deconvolution method for noise, we performed recovery of the oxygen histogram from the same oxygen distribution with varying SNR in the simulated photometric signal. The detrimental effects of decreasing SNR on the deconvolution appear to be modest (Fig. 4), and there is a good resemblance between the theoretical histogram and recovered histograms for SNRs of 20 and higher. In practice, SNR is dependent on the number of averaged laser pulses. For the in vivo condition we used an averaged photometric signal consisting of 64 delayed fluorescence traces, resulting in an SNR that easily exceeded a value of 40. The SNR for the isolated liver experiments was ~30.

To test the stability of the histogram fitting procedure in terms of reproducibility with slightly altered noise, several simulated photometric signals from the same underlying oxygen distribution (but with newly generated noise patterns) were sequentially analyzed (Fig. 5). The fitting procedure is stable and does not show severe deformations of the histogram in sequential runs, and the SD in the bins of the mean histogram is very small (even at $n = 3$).

Mitochondrial oxygen distributions in vivo are unknown and cannot a priori be assumed to be Gaussian. Therefore, it is essential for the histogram fitting procedure to be capable of recovering complex distributions. Although the deconvolution method in itself does not assume any underlying distribution, the Marquart-Levenberg algorithm requires an initial guess of the fitting parameters. To avoid biasing the outcome of the fit in any particular direction, the initial guess parameters for the weight factors were all set to 0.1 (i.e., corresponding to a flat distribution). Examples of several simulated complex oxygen distributions and their retrieval by the deconvolution method are provided in Fig. 6. It is clear that the histogram fitting procedure is not limited to Gaussian distributions and can provide insight into complex underlying oxygen distributions.

In vitro calibration constants are valid in intact tissue

We tested the validity of the calibration in isolated cells for intact liver tissue. To this end, isolated perfused rat livers were used 2 h after ALA infusion. The oxygen dependence of the delayed fluorescence signal is clearly demonstrated in a liver that was unintentionally inhomogeneously perfused (Fig. 7 *a*). One lobe appeared lighter than the rest of the liver with a surface temperature that was 2°C lower, indicative of inadequate perfusion. During perfusion with carbogen-saturated

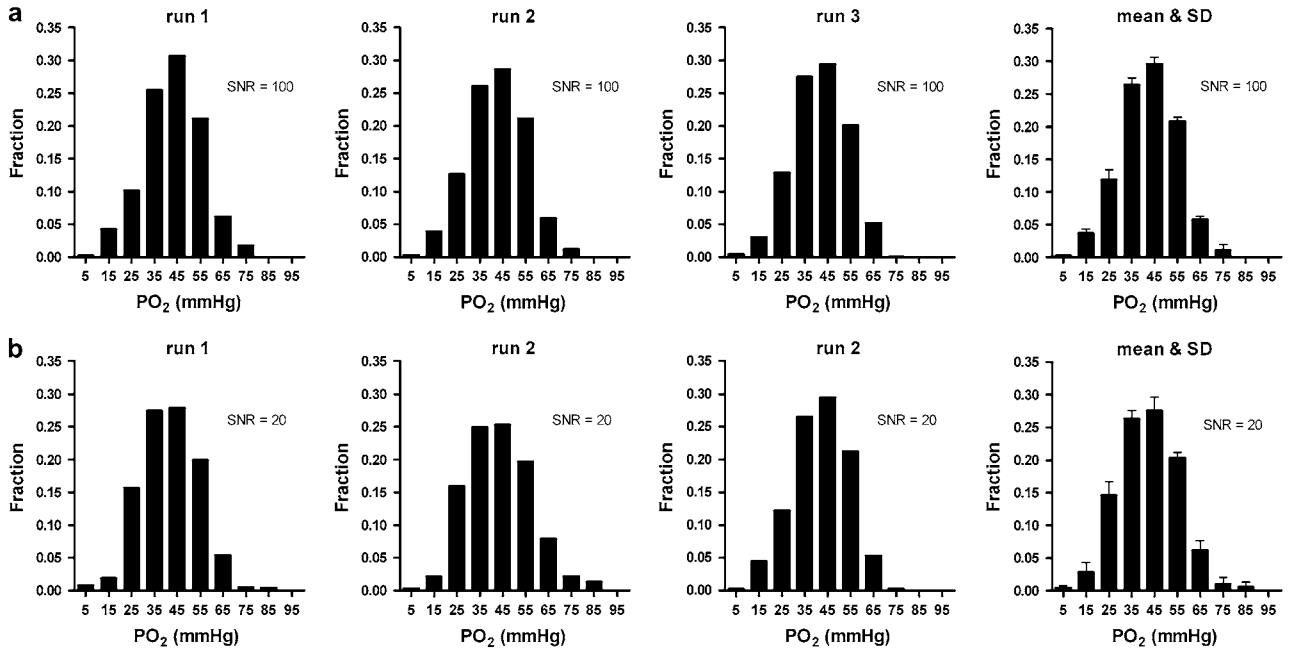

FIGURE 5 Stability of the histogram fitting procedure in recovery of the underlying PO_2 histogram with altered random noise. (*a*) Sequential runs at an SNR of 100. (*b*) Sequential runs at an SNR of 20. The underlying oxygen distribution is the same as in Fig. 1.

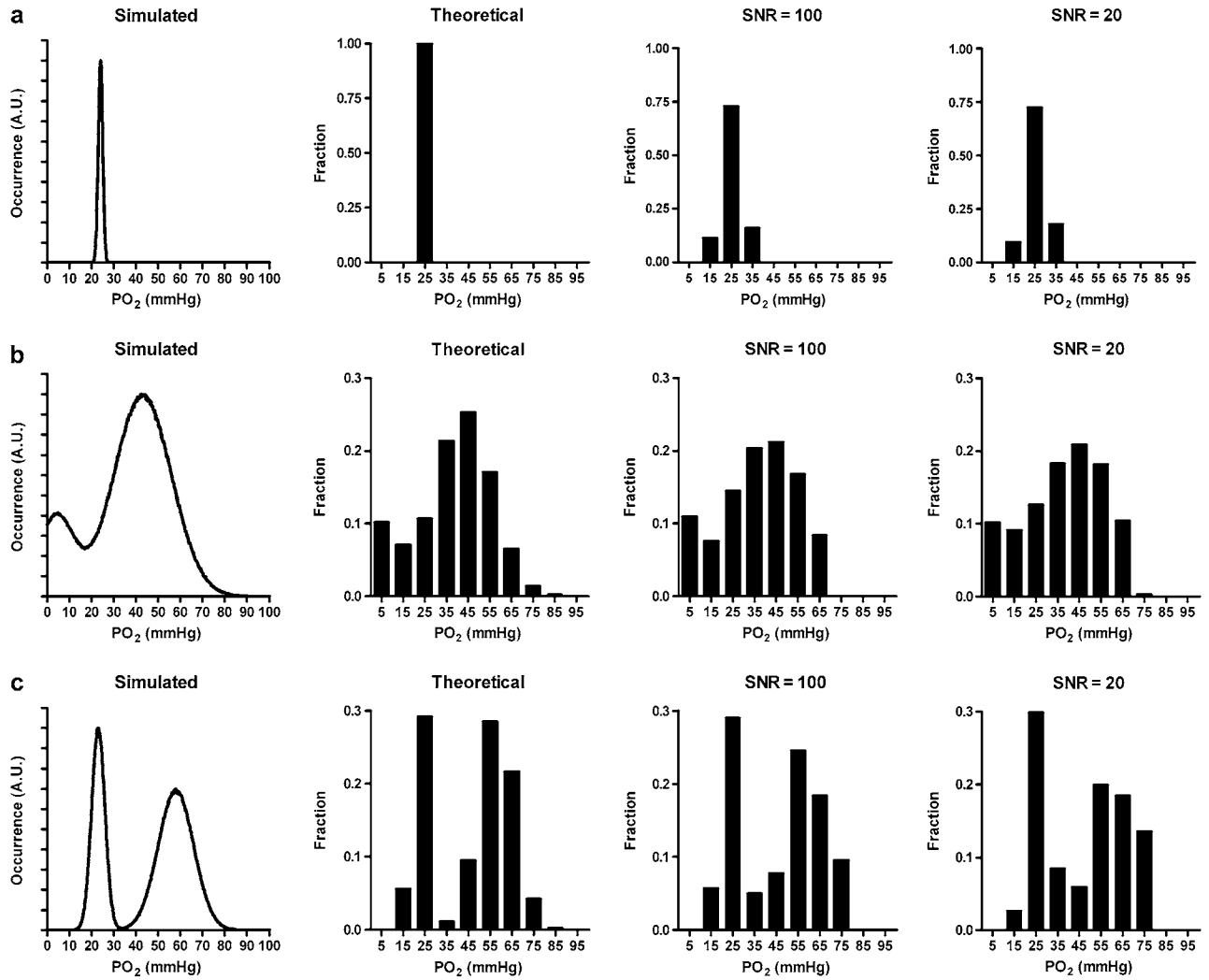

FIGURE 6 Recovery of various shapes of oxygen histograms and the effect of altered SNR.

(95% oxygen, 5% carbon dioxide) perfusate, the delayed fluorescence lifetime in the less-perfused part of the liver was much longer (205 μs) than that in the well-perfused part (74 μs). Blockage of oxygen consumption consistently led to a decrease in delayed fluorescence lifetime corresponding to an increase in PO_2 (see Fig. 7 *b* for an example).

To test the calibration constants, delayed fluorescence was measured at various fixed oxygen concentrations in the perfusate, before and after blockage of cellular oxygen consumption in a series of isolated liver experiments. Regardless of the oxygen concentration in the perfusate, the baseline mitochondrial PO_2 ($PO_{2,mito}$) was ~20 mmHg (Fig. 7 *c*). The relatively low PO_2 values at baseline reflect the PO_2 gradient between the perfusate and the mitochondria. The PO_2 values measured after blockage of cellular respiration corresponded well to theoretically expected values. These experiments also demonstrate that the measurement is not dependent on the presence of blood, indicating that the signal truly originates from the tissue. This is in concordance with our observation that no delayed fluorescence was detected from whole blood or plasma, in agreement with the time course of previously reported PpIX kinetics (20).

The isolated organ is also a valuable model to test the algorithm for recovery of oxygen distributions in practice, since blockage of cellular respiration should ideally lead to a small distribution around the preset PO_2 value. The applied method for lifetime deconvolution was very effective in indicating the correct PO_2 bin (Fig. 7, *d–f*). The slight broadening of the peak can be attributed to residual noise in the signal, and it is likely that some residual oxygen heterogeneity was present in the tissue. The surface of the livers was not isolated from air, so it is likely that a contribution to higher PO_2 bins is due to the presence of atmospheric oxygen.

In vivo measurement of mitoPO_2 and its heterogeneity

To test the sensitivity and applicability of the delayed fluorescence lifetime technique under relevant pathophysiologi-

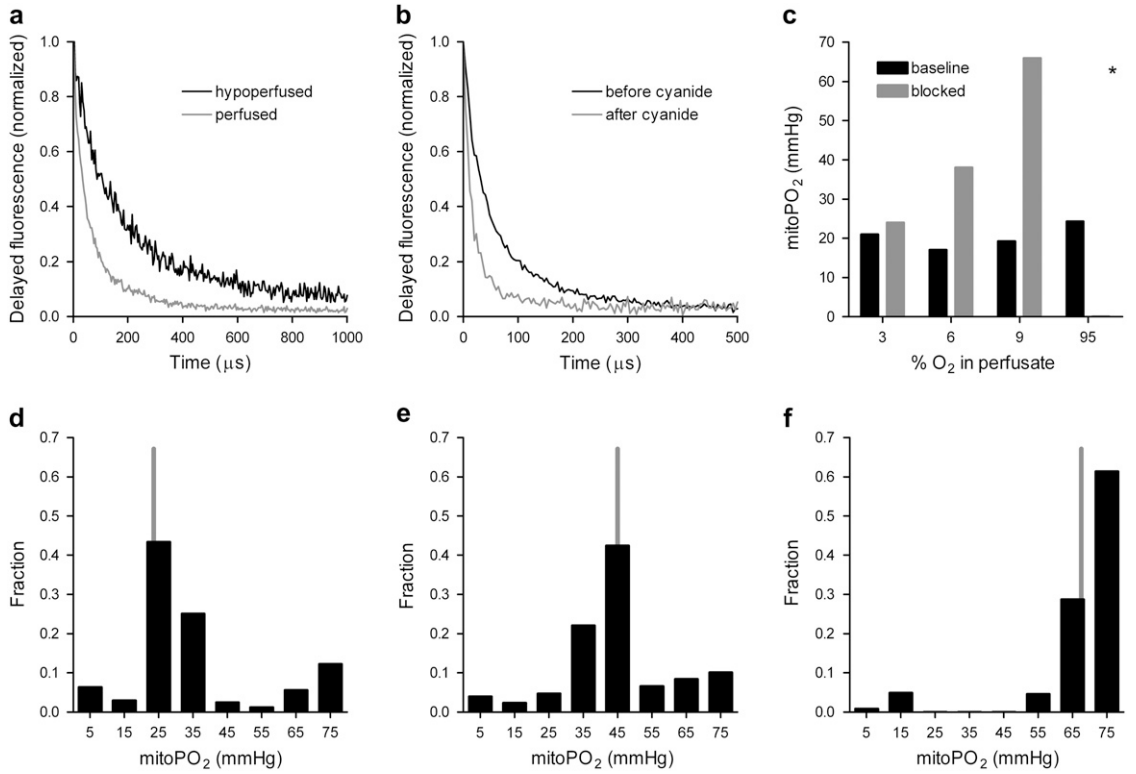

FIGURE 7 PpIX delayed fluorescence from intact rat liver has the same oxygen-dependent properties as in isolated cells. (*a*) Delayed fluorescence traces from a normally perfused and a hypoperfused area of an isolated rat liver. (*b*) Delayed fluorescence traces from an isolated liver before and after blockage of cellular respiration. (*c*) Mitochondrial PO_2 measured in isolated rat liver before (baseline) and after blocking of cellular respiration using the calibration constants from the cell suspension experiments. Shown are the results of four individual livers. *Lifetime too short to be accurately measured with current setup. (*d–f*) Distributions of mitoPO_2 after blockage of respiration at 3% oxygen (*d*), 6% oxygen (*e*), and 9% oxygen (*f*) in the perfusate. The shaded line denotes the theoretically expected value.

cal conditions, we varied FiO_2 in one group of rats and induced ischemia-reperfusion in another group of animals. Two hours after ALA administration, we observed a clear oxygen-dependent delayed fluorescence signal from rat liver in vivo (Fig. 8 *a*). We performed a series of experiments with stepwise variation in FiO_2 concentration (Fig. 8 *b*). The average measurements, obtained by monoexponential fitting of the signal, were highly reproducible in value, with low variance between rats. Notably, mitoPO_2 was especially sensitive to small changes in FiO_2 around atmospheric oxygen levels (20% inspired oxygen). The recovery of mitoPO_2 histograms (Fig. 8, *c–h*) provides a more detailed view on the effects of FiO_2 on cellular oxygenation. At $FiO_2 \geq 20\%$, mitoPO_2 is approximately normally distributed, in good agreement with previous invasive micro oxygen electrode measurements (21). However, even a mild reduction of FiO_2 to 18% resulted in severe skewing of the mitoPO_2 distribution toward low PO_2. It is interesting that although further reduction of FiO_2 results in overall lower mitoPO_2, mitoPO_2 is relatively preserved in the 15 mmHg bin (representing 10–20 mmHg) (Fig. 8, *g* and *h*).

In another group of animals we performed a short ischemia-reperfusion protocol consisting of 30 min of ischemia followed by 15 min of reperfusion (Fig. 9 *a*). Overall mitoPO_2 dropped to ~10 mmHg during ischemia, and then recovered to approximately baseline after the 15-min reperfusion (Fig. 9 *b*). Again the mitoPO_2 histograms provide valuable additional information (Fig. 9, *c–g*). Similar to the condition of breathing a low FiO_2, a large part of the signal originated from mitochondria in the 15 mmHg bin. Apparently, the liver in vivo was not completely anoxic during ischemia. Since this appears counterintuitive, it should be stressed that this finding was not caused by a limitation of our technique: longer lifetimes (lower PO_2) were measured in both isolated hepatocytes and isolated liver under forced oxygen depletion. Moreover, in previously reported tissue PO_2 measurements, ischemia did not reduce tissue PO_2 under 14 mmHg (21). Reperfusion led to complete alteration of the mitoPO_2 distribution, which flattened overall compared to the baseline situation (Fig. 9, *f* and *g*). Both low- and high-mitoPO_2 regions were more prominently present, with some development toward higher PO_2 during progress of reperfusion.

Influence of out-of-range PO_2 on histogram recovery

The choice of bin width and number of bins limits our current implementation of the deconvolution method to PO_2 values

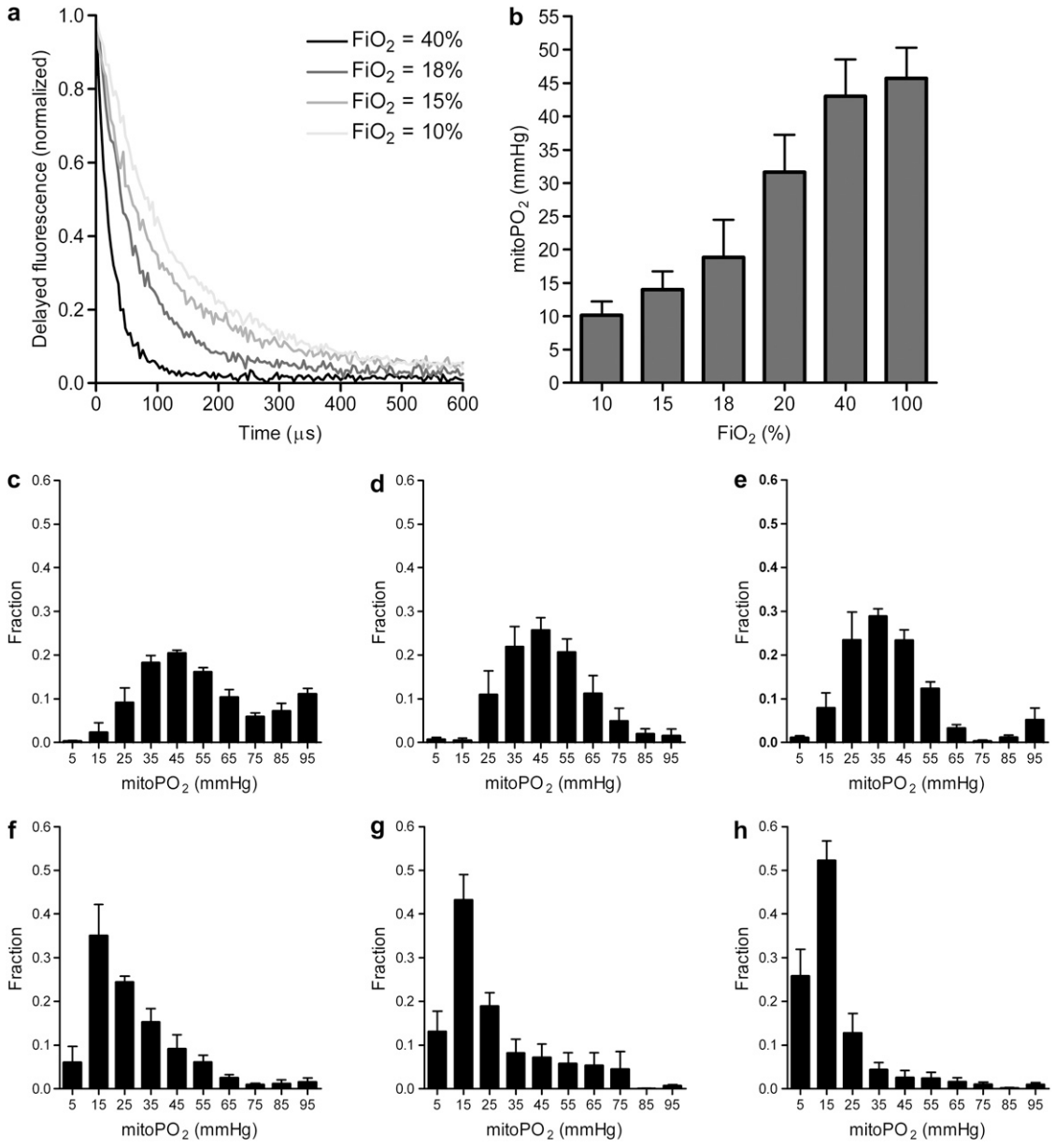

FIGURE 8 Delayed fluorescence lifetime measurements can be used for quantitative assessment of in vivo mitoPO$_2$. Measurements in rat liver in vivo are shown. (*a*) Normalized delayed fluorescence lifetime signals different FiO$_2$ concentrations. (*b*) Average mitoPO$_2$ measured versus the FiO$_2$. Error bars indicate the SD ($n = 6$). (*c–h*) Distributions of mitoPO$_2$ at different FiO$_2$ concentrations: 100% O$_2$ (*c*), 40% O$_2$ (*d*), 20% O$_2$ (*e*), 18% O$_2$ (*f*), 15% O$_2$ (*g*), and 10% O$_2$ (*h*).

between 0 and 100 mmHg. For in vivo application of the delayed fluorescence lifetime technique under physiological circumstances, this can be considered an adequate range. However, a contribution of room air to the oxygenation of superficial tissue layers cannot be excluded, and therefore it is possible that PO_2 values above 100 mmHg are present in the measurement volume. The short lifetimes from regions with a PO_2 above 100 mmHg are not represented in the fit algorithm and therefore might lead to instability or an adverse effect on the shape of recovered histograms. Therefore, we tested in computer simulations the effect of adding high PO_2 values (around those of room air) on the histogram fitting procedure. PO_2 values outside the range of the deconvolution method induce the occurrence of small peaks at the high PO_2 bins (Fig. 10). The accurate recovery of the remaining distribution is not affected.

Effect of ambient oxygen on mitoPO$_2$ histograms in vivo

The previous computer simulations demonstrated that PO_2 values outside the range of the deconvolution method are represented as contributions to the highest PO_2 bins. It is important that the recovery of the ''true'' oxygen histo-

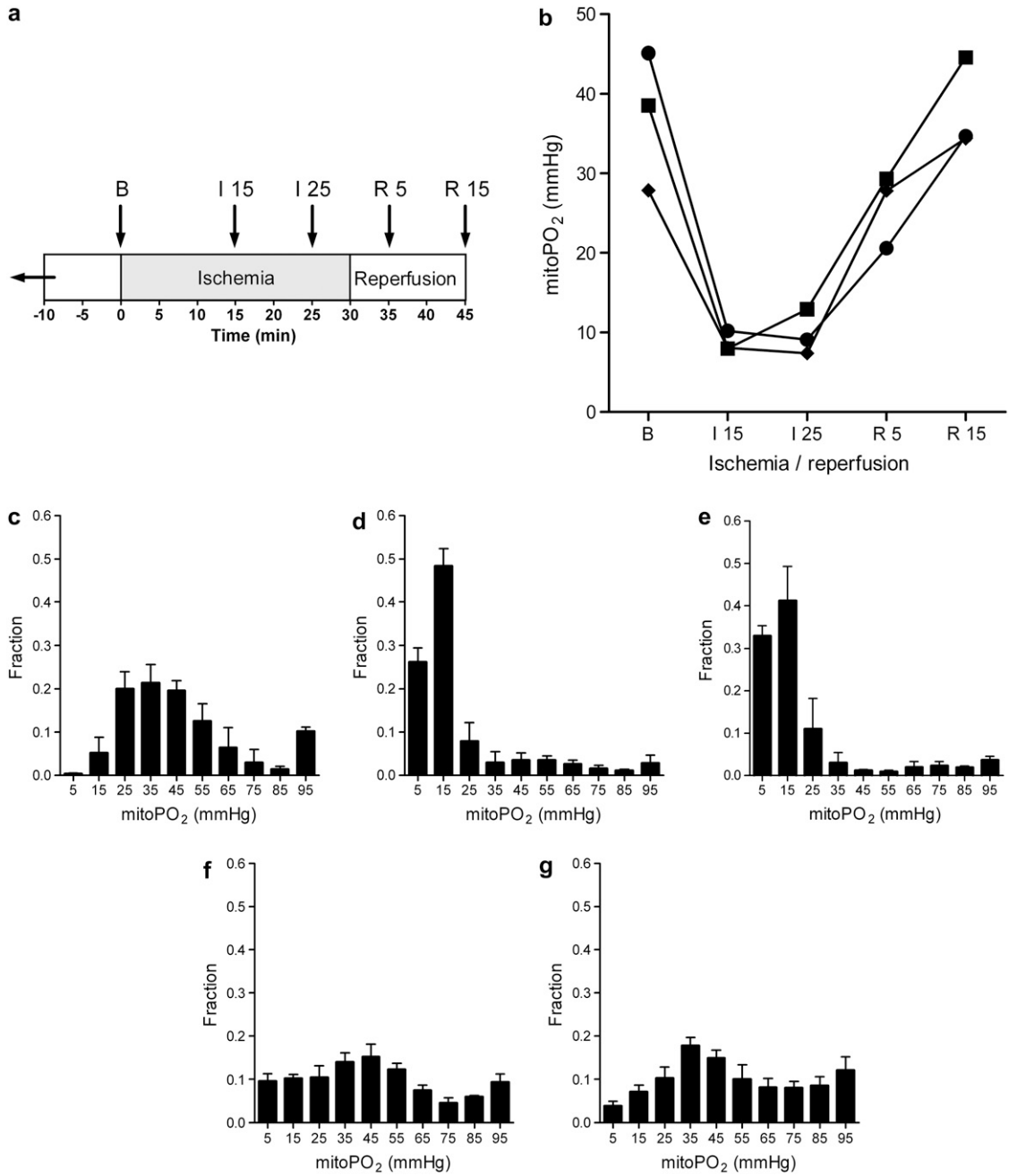

FIGURE 9 Effect of ischemia-reperfusion on mitoPO$_2$ in rat liver in vivo. (*a*) Ischemia-reperfusion protocol and times of measurement: baseline (B), 15 (I 15) and 25 (I 25) min ischemia, and 5 (R 5) and 15 (R 15) min reperfusion. (*b*) Average mitoPO$_2$. (*c–g*) Distributions of mitoPO$_2$ at time points B (*c*), I 15 (*d*), I 25 (*e*), R 5(*f*), and R 15 (*g*). Error bars indicate the SD ($n = 3$).

gram was not affected. However, the situation in real life is more complex. Here, exposure of the organ surface to ambient air could cause the presence of nonphysiological high oxygen concentrations. Diffusion of oxygen out of this high-PO$_2$ region into low-PO$_2$ regions could cause disturbance of the oxygen distribution in the tissue and therefore affect the recovered mitoPO$_2$ histogram. To investigate the occurrence of this effect and to quantify its possible influence, we performed in vivo experiments ($n = 5$) in which the surface oxygen concentration was altered by blowing prewarmed and humidified gas mixtures over the surface of the liver at a rate of 250 mL/min (Fig. 11). The presence of 10% and 20% oxygen at the surface is visible as small contributions to the highest PO$_2$ bins. However, the remaining mitoPO$_2$ histograms are not affected, indicating that only a small (the most superficial) part of the measurement volume is influenced by the oxygen concentration at the organ surface.

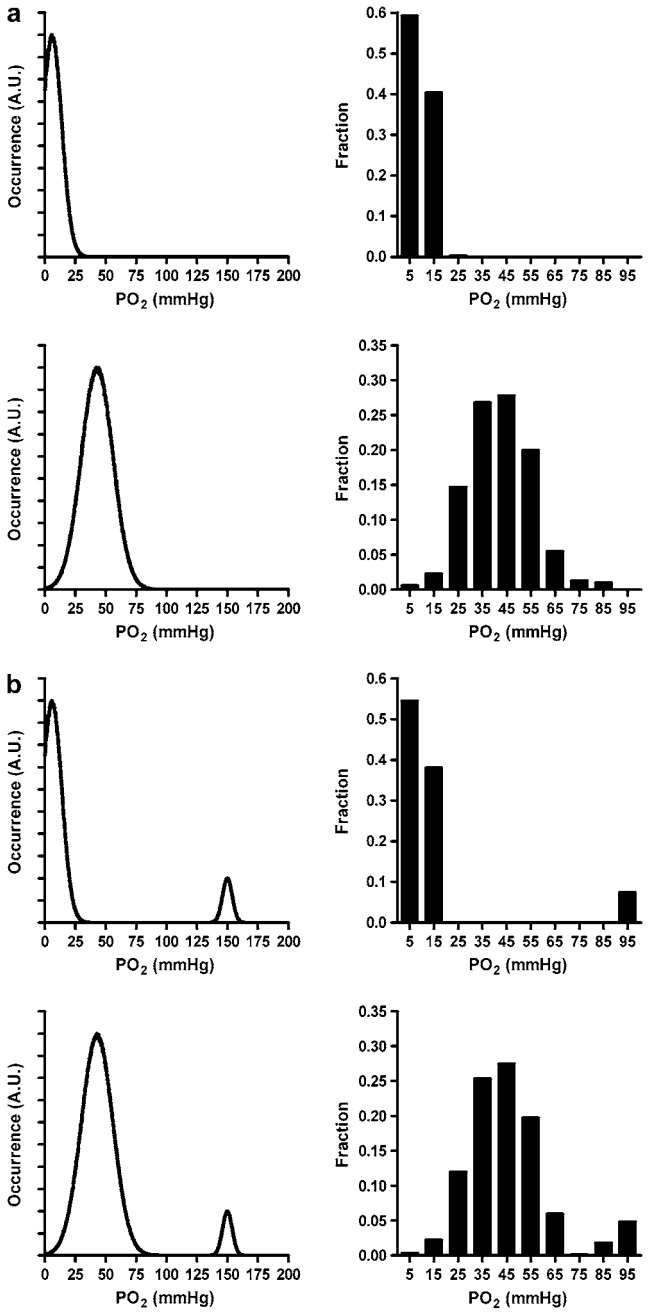

FIGURE 10 Effect of the presence of a region with PO_2 outside the range covered by the deconvolution method. (*a*) Two simulated PO_2 distributions and their recovery from the simulated photometric signal. (*b*) Effect of the presence of a small peak at ~150 mmHg (mimicking the effect of room air).

Effect of PpIX enhancement on oxygen metabolism

To test whether ALA-induced enhancement of mitochondrial PpIX levels changed oxygen metabolism, we conducted a series of respiration experiments in isolated mitochondria. Delayed fluorescence was readily observed from suspensions of mitochondria isolated from rats after ALA administration (Fig. 12 *a*). This finding confirms the mitochondrial localization of PpIX and shows that PpIX is not removed by the isolation procedure. The presence of ALA-induced PpIX had no effects on state 3 and 4 respiration, or on the RCI and ADP:O ratio compared to control rats (Fig. 12 *b*).

DISCUSSION

We have reported the development and application of a technique that enables the measurement of mitoPO_2 and the assessment of its heterogeneity in vivo by delayed fluorescence quenching of endogenously synthesized PpIX. The power of the technique and its potential for a broad field of applications are due to the combination of a specific and robust lifetime technique with reliance on an endogenous compound.

This approach has several distinct advantages. In the context of oxygen measurements, it is the first technique that allows quantitative PO_2 measurements to be obtained at the mitochondrial level in vivo. Unlike existing techniques for in vivo oxygen measurements (5), it does not require tissue destruction or injection of exogenous oxygen-sensitive compounds. The ability to recover mitoPO_2 histograms with high temporal resolution (on the order of seconds) is clearly advantageous. There are several deconvolution techniques available, each of which has specific advantages and disadvantages. For example, the maximum entropy method (22) allows very detailed recovery of oxygen histograms (resolving typically 200 lifetimes) but requires very high SNR levels for stable operation. The use of such a deconvolution technique for the recovery of oxygen histograms in the setting of phosphorescence lifetime measurements was recently questioned due to the occurrence of nonphysiological high PO_2 values (23); however, this effect was proposed to result from blurring of the high-PO_2 region due to diminished contribution of short lifetimes to the overall phosphorescence signal (24,25) (decreasing the SNR for high-PO_2 regions). The method we chose operates stably at modest SNRs, but at the expense of a reduced resolving power (11). Nevertheless, this approach allows insight into complex oxygen distributions in tissue samples, as demonstrated by its practical application and in computer simulations. Since the isolated and in vivo livers were not shielded from room air, it is likely that atmospheric oxygen caused some of the high values for mitoPO_2. Indeed, in computer simulations, the addition of room air caused high PO_2 bins to occur without affecting the underlying PO_2 distribution. Furthermore, in vivo experiments clearly demonstrated the influence of ambient oxygen concentration on mitoPO_2. Although in our current setting this had no detrimental effects on the underlying mitoPO_2 distribution, it is important to note that the influence of ambient oxygen might be present in any type of (oxygen) measurement that is limited in penetration depth. It should be noted, however, that covering the organ surface with Saran Wrap or keeping the oxygen concentration at the surface artificially low might equally well deviate from the physiological in vivo situation.

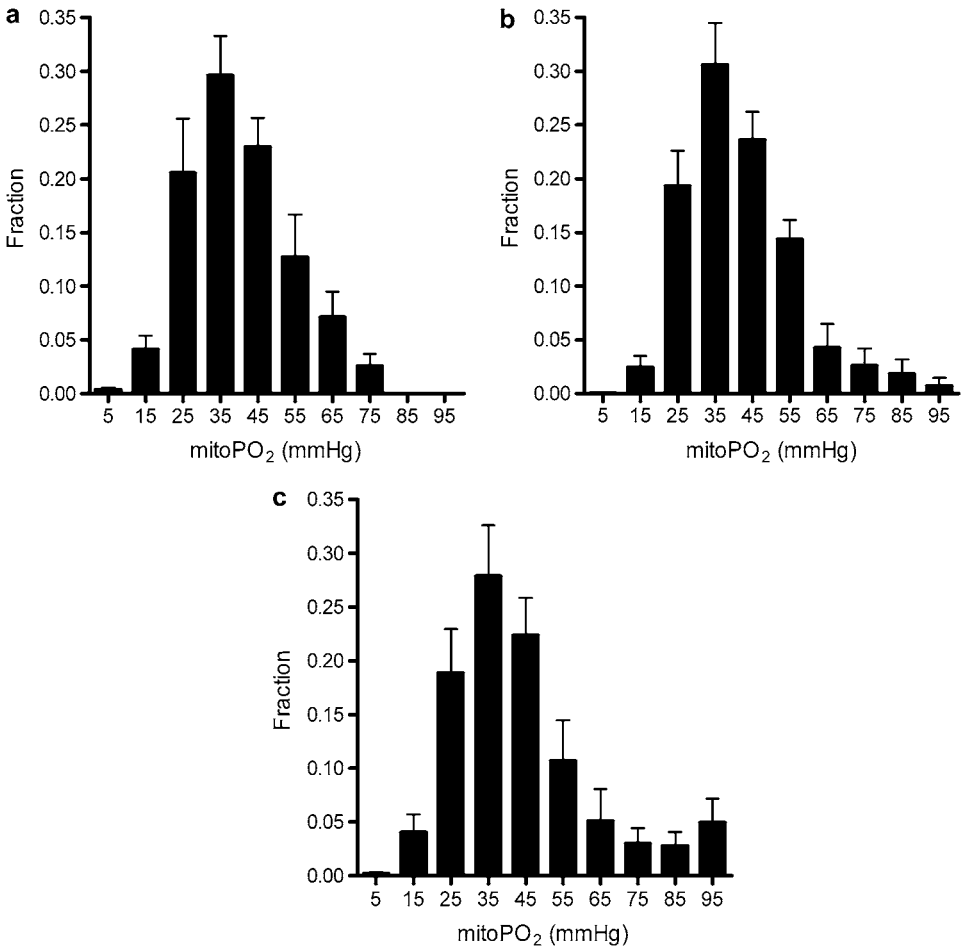

FIGURE 11 Effect of the oxygen concentration in the ambient atmosphere on the mitoPO$_2$ histograms. (*a*) The measured oxygen concentration at the surface was 1.2% ± 0.4%. (*b*) The measured oxygen concentration at the surface was 10.0% ± 0.7%. (*c*) The measured oxygen concentration at the surface was 20.2% ± 0.8%. Error bars indicate the SD ($n = 5$).

Although deconvolution techniques allow measurement of oxygen heterogeneity with high temporal resolution, for insights into the nature of this heterogeneity, and its relation to localization, other techniques have to be explored. Since it is an optical technique, delayed fluorescence of PpIX could well be combined with microscopic setups to increase the spatial resolution to allow the unraveling of tissue oxygenation on the micron scale. For example, two-photon excitation (26) provides three-dimensional insight into oxygen distributions, and intravital microscopy (27–30) provides anatomical information. Finally, for in vivo measurements, another crucial factor is that lifetime measurements are not disturbed by changes in tissue optical properties.

Although PpIX is endogenously present, its normal levels are very low. Therefore, to improve its detection our current approach relies on the application of its precursor, ALA, to enhance mitochondrial PpIX levels. Although ALA is nontoxic and is used in daily clinical practice in photodynamic therapy (31) and photodynamic diagnosis (32), high levels of PpIX are not harmless. Under the conditions in our study, we found no effects of ALA-induced PpIX levels on mitochondrial respiration. However, in general, the concentrations of ALA or incubation times that can be used safely without changing tissue metabolism remain to be determined. Excitation of PpIX is known to induce apoptosis in cells as a result of oxygen-radical formation (31). We did not detect any significant changes in cell survival after repeated illumination in ALA-treated cell cultures (10). The excitation light levels needed for mitoPO$_2$ measurements are orders of magnitude less than light levels used in photodynamic therapy, and therefore tissue damage due to phototoxicity may not be a problem in practice. Nevertheless, we would like to point out that for any intended application (especially if aimed at clinical use), an appropriate risk and safety assessment is required because of potential phototoxicity. Especially, one should strive to minimize the cumulative dose of excitation light to avoid induction of apoptosis.

It is interesting that the values of in vivo mitoPO$_2$ are in the range of reported hepatic tissue PO$_2$ values (21,33). This indicates that in the liver in vivo, the final diffusion gradient from the microcirculation to the mitochondria is quite small. Apparently, the hepatic architecture does not induce a profound diffusion barrier, since the intracellular oxygen gradient is only a few mmHg (10). Indeed, a sinusoidal-to-cell PO$_2$ gradient of ~5 mmHg was previously reported (34).

The finding of high hepatic mitoPO$_2$ values in vivo is of significant interest. Whether molecular oxygen plays a role in the regulation of cellular metabolism has long been a subject

a

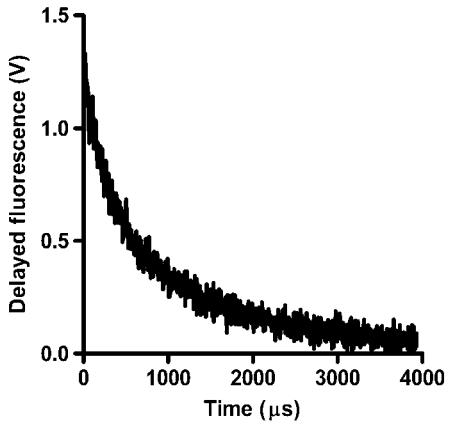

b

	Control	ALA	p-value
State 3	80.3 ± 15.9 *	85.4 ± 10.3 *	0.61
State 4	14.1 ± 3.4 *	14.5 ± 1.5 *	0.81
RCI	5.8 ± 0.5	5.9 ± 0.5	0.72
ADP/O	2.0 ± 0.1	2.0 ± 0.1	1.00

* respiratory rate in nmol $O_2 \cdot min^{-1} \cdot mg\ protein^{-1}$

FIGURE 12 Mitochondrial oxygen metabolism is not affected by the presence of ALA-induced PpIX. (*a*) Delayed fluorescence signal observed from a deoxygenated suspension of isolated rat liver mitochondria. (*b*) State 3 and 4 respiration, RCI, and ADP:O ratio in freshly isolated rat liver mitochondria from control rats and rats receiving 200 mg/kg ALA. Mean and SD from four control animals and four ALA-treated animals.

of debate. Classical studies in isolated mitochondria and cells have shown that the respiration rate is unaffected by oxygen levels until PO_2 levels drop below 2–3 mmHg (35–38). This indicates a lack of metabolic control, under the assumption that normal physiological intracellular PO_2 may be well above this threshold level. Alternatively, it has been stated that the general view of mitochondrial function is biased owing to the excessively high PO_2 (air-saturated, i.e., ~150 mmHg) range in most in vitro experiments (39), assuming physiological normoxic mitochondrial PO_2 to be below 1 kPa (7.5 mmHg). In skeletal muscle, a combination of myoglobin saturation, phosphorylation state, and intracellular pH measurements led to the rejection of the hypothesis that oxygen plays a regulatory role in cellular respiration (40). However, recent studies have questioned the idea that oxygen acts as a simple substrate over the physiological range of oxygen tensions, and have identified a mechanism in hepatocytes called the ''oxygen conformance of metabolism'' (41,42). Here oxygen consumption is downregulated when cells are subjected to moderate oxygen deprivation for extended periods of time (41). Of interest is that this phenomenon already occurs at relatively high PO_2 values of ~70 mmHg (4,42). The data presented here provide new insights into this possible mechanism by identifying the hepatic mitochondrial PO_2 in vivo to be in the range of this oxygen conformance of metabolism. This makes it very likely that metabolic control by oxygen, as demonstrated in vitro, is a cellular regulation mechanism acting under normal physiological circumstances and is not limited to pathophysiological states of hypoxia. Since the mitochondria are considered to play a major role in cellular oxygen sensing (3), knowledge of in vivo mitochondrial PO_2 levels provides a sound basis for future in vitro experiments.

CONCLUSIONS

This delayed fluorescence lifetime approach manifests potent abilities for the quantitative assessment of mitochondrial oxygen tension in vivo. In ALA-treated rats, oxygen-dependent delayed fluorescence was emitted by many tissues and was calibrated in isolated hepatocytes and isolated livers. In combination with a lifetime-deconvolution algorithm, this allowed the measurement of mitoPO_2 histograms in rat liver in vivo. Because the technique relies on enhancement of an endogenously synthesized porphyrin, it is in principle usable in humans. If its safety in terms of phototoxicity can be proven, it may be possible to assess mitoPO_2 in the clinical setting. The technique is expected to provide the basis of many new applications for mitochondrial PO_2 measurements, including transplantation research, intensive-care research, and tissue engineering.

This work was supported in part by a Technological Collaboration Grant (TSGE 1048) from the Dutch Ministry of Economic Affairs. As part of this collaboration, K. Boller and A.F. Niewenhuis (Department of Laser Physics and Non-linear Optics, University of Twente, Enschede, The Netherlands) kindly provided the pulsed laser system, the tunable optical parametric oscillator, and technical assistance. J. Stap was funded in part by a grant from the Dutch Cancer Society.

E.G.M. conceived and designed the study, performed experiments, programmed the software, performed the computer simulations, and wrote the manuscript; T.J. and C.J.Z. were involved in the design of biological experiments, performed experiments, and assisted with the interpretation of data and drafting of the manuscript. A.H. and C.J.Z. performed the mitochondrial respiration experiments. J.H.P.M.H.-W. assisted with the isolated liver experiments and performed the isolation of hepatocytes; G.M.B. assisted with in vivo experiments; J.S. performed fluorescence microscopy; J.F.B. was involved in the construction of the delayed fluorescence setup; and C.I. facilitated the study and supervised the work.

REFERENCES

1. Mitchell, P., and J. Moyle. 1967. Chemiosmotic hypothesis of oxidative phosphorylation. *Nature*. 213:137–139.
2. Chandel, N. S., G. R. Budinger, S. H. Choe, and P. T. Schumacker. 1997. Cellular respiration during hypoxia. Role of cytochrome oxidase as the oxygen sensor in hepatocytes. *J. Biol. Chem.* 272:18808–18816.
3. Kemp, P. J. 2006. Detecting acute changes in oxygen: will the real sensor please stand up? *Exp. Physiol.* 91:829–834.
4. Rissanen, E., H. K. Tranberg, and M. Nikinmaa. 2006. Oxygen availability regulates metabolism and gene expression in trout hepatocyte cultures. *Am. J. Physiol. Regul. Integr. Comp. Physiol.* 291: R1507–R1515.

5. Springett, R., and H. M. Swartz. 2007. Measurements of oxygen *in vivo*: overview and perspectives on methods to measure oxygen within cells and tissues. *Antioxid. Redox Signal.* 9:1295–1301.
6. Whalen, W. J., P. Nair, and R. A. Ganfield. 1973. Measurements of oxygen tension in tissues with a micro oxygen electrode. *Microvasc. Res.* 5:254–262.
7. Rumsey, W. L., J. M. Vanderkooi, and D. F. Wilson. 1988. Imaging of phosphorescence: a novel method for measuring oxygen distribution in perfused tissue. *Science.* 241:1649–1651.
8. Vanderkooi, J. M., G. Maniara, T. J. Green, and D. F. Wilson. 1987. An optical method for measurement of dioxygen concentration based upon quenching of phosphorescence. *J. Biol. Chem.* 262:5476–5482.
9. Swartz, H. M., and R. B. Clarkson. 1998. The measurement of oxygen *in vivo* using EPR techniques. *Phys. Med. Biol.* 43:1957–1975.
10. Mik, E. G., J. Stap, M. Sinaasappel, J. F. Beek, J. A. Aten, T. G. van Leeuwen, and C. Ince. 2006. Mitochondrial PO_2 measured by delayed fluorescence of endogenous protoporphyrin IX. *Nat. Methods.* 3:939–945.
11. Golub, A. S., A. S. Popel, L. Zheng, and R. N. Pittman. 1997. Analysis of phosphorescence in heterogeneous systems using distributions of quencher concentration. *Biophys. J.* 73:452–465.
12. Johannes, T., E. G. Mik, and C. Ince. 2006. Dual-wavelength phosphorimetry for determination of cortical and subcortical microvascular oxygenation in rat kidney. *J. Appl. Physiol.* 100:1301–1310.
13. Poulson, R. 1976. The enzymic conversion of protoporphyrinogen IX to protoporphyrin IX in mammalian mitochondria. *J. Biol. Chem.* 251:3730–3733.
14. Fukuda, H., A. Casas, and A. Batlle. 2005. Aminolevulinic acid: from its unique biological function to its star role in photodynamic therapy. *Int. J. Biochem. Cell Biol.* 37:272–276.
15. Dalton, J., C. A. McAuliffe, and D. H. Slater. 1972. Reaction between molecular oxygen and photo-excited protoporphyrin IX. *Nature.* 235:388.
16. Heijnen, B. H., S. Q. van Veen, I. H. Straatsburg, and T. M. van Gulik. 2001. Pronounced effect of minor changes in body temperature on ischemia and reperfusion injury in rat liver. *J. Appl. Physiol.* 91:265–268.
17. Mik, E. G., C. Donkersloot, N. J. Raat, and C. Ince. 2002. Excitation pulse deconvolution in luminescence lifetime analysis for oxygen measurements in vivo. *Photochem. Photobiol.* 76:12–21.
18. Groen, A. K., H. J. Sips, R. C. Vervoorn, and J. M. Tager. 1982. Intracellular compartmentation and control of alanine metabolism in rat liver parenchymal cells. *Eur. J. Biochem.* 122:87–93.
19. Heinen, A., A. K. Camara, M. Aldakkak, S. S. Rhodes, M. L. Riess, and D. F. Stowe. 2007. Mitochondrial Ca2+-induced K+ influx increases respiration and enhances ROS production while maintaining membrane potential. *Am. J. Physiol. Cell Physiol.* 292:C148–C156.
20. van den Boogert, J., R. van Hillegersberg, F. W. de Rooij, R. W. de Bruin, A. Edixhoven-Bosdijk, A. B. Houtsmuller, P. D. Siersema, J. H. Wilson, and H. W. Tilanus. 1998. 5-Aminolaevulinic acid-induced protoporphyrin IX accumulation in tissues: pharmacokinetics after oral or intravenous administration. *J. Photochem. Photobiol. B.* 44:29–38.
21. van Wagensveld, B. A., T. M. van Gulik, E. E. Gabeler, A. J. van der Kleij, H. Obertop, and D. J. Gouma. 1998. Intrahepatic tissue PO_2 during continuous or intermittent vascular inflow occlusion in a pig liver resection model. *Eur. Surg. Res.* 30:13–25.
22. Vinogradov, S. A., and D. F. Wilson. 2000. Recursive maximum entropy algorithm and its application to the luminescence lifetime distribution recovery. *Appl. Spectrosc.* 54:849–855.
23. Tsai, A. G., P. Cabrales, P. C. Johnson, and M. Intaglietta. 2007. New phosphorescence quenching oxygen measurements technique yields unusual tissue and plasma PO_2 distributions. *J. Appl. Physiol.* 102: 2081–2082.
24. Wilson, D. F., W. M. F. Lee, S. Makonnen, O. Finikova, S. Apreleva, and S. A. Vinogradov. 2007. Reply to Tsai, Cabrales, Johnson, and Intaglietta. *J. Appl. Physiol.* 102:2083.
25. Wilson, D. F., W. M. Lee, S. Makonnen, O. Finikova, S. Apreleva, and S. A. Vinogradov. 2006. Oxygen pressures in the interstitial space and their relationship to those in the blood plasma in resting skeletal muscle. *J. Appl. Physiol.* 101:1648–1656.
26. Mik, E. G., T. G. van Leeuwen, N. J. Raat, and C. Ince. 2004. Quantitative determination of localized tissue oxygen concentration in vivo by two-photon excitation phosphorescence lifetime measurements. *J. Appl. Physiol.* 97:1962–1969.
27. Cabrales, P., A. G. Tsai, and M. Intaglietta. 2008. Modulation of perfusion and oxygenation by red blood cell oxygen affinity during acute anemia. *Am. J. Respir. Cell Mol. Biol.* 38:354–361.
28. Golub, A. S., M. C. Barker, and R. N. Pittman. 2007. PO_2 profiles near arterioles and tissue oxygen consumption in rat mesentery. *Am. J. Physiol. Heart Circ. Physiol.* 293:H1097–H1106.
29. Smith, L. M., A. S. Golub, and R. N. Pittman. 2002. Interstitial PO_2 determination by phosphorescence quenching microscopy. *Microcirculation.* 9:389–395.
30. Tsai, A. G., B. Friesenecker, M. C. Mazzoni, H. Kerger, D. G. Buerk, P. C. Johnson, and M. Intaglietta. 1998. Microvascular and tissue oxygen gradients in the rat mesentery. *Proc. Natl. Acad. Sci. USA.* 95:6590–6595.
31. Peng, Q., T. Warloe, K. Berg, J. Moan, M. Kongshaug, K. E. Giercksky, and J. M. Nesland. 1997. 5-Aminolevulinic acid-based photodynamic therapy. Clinical research and future challenges. *Cancer.* 79:2282–2308.
32. Kelty, C. J., N. J. Brown, M. W. Reed, and R. Ackroyd. 2002. The use of 5-aminolaevulinic acid as a photosensitiser in photodynamic therapy and photodiagnosis. *Photochem. Photobiol. Sci.* 1:158–168.
33. Uhlmann, D., U. C. Pietsch, S. Ludwig, J. Hess, B. Armann, G. Gaebel, E. Escher, L. Schaffranietz, A. Tannapfel, M. Fiedler, J. Hauss, and H. Witzigmann. 2004. Assessment of hepatic ischemia-reperfusion injury by simultaneous measurement of tissue PO_2, PCO_2, and pH. *Microvasc. Res.* 67:38–47.
34. Kekonen, E. M., V. P. Jauhonen, and I. E. Hassinen. 1987. Oxygen and substrate dependence of hepatic cellular respiration: sinusoidal oxygen gradient and effects of ethanol in isolated perfused liver and hepatocytes. *J. Cell. Physiol.* 133:119–126.
35. Longmuir, I. S. 1957. Respiration rate of rat-liver cells at low oxygen concentrations. *Biochem. J.* 65:378–382.
36. Wilson, D. F., W. L. Rumsey, T. J. Green, and J. M. Vanderkooi. 1988. The oxygen dependence of mitochondrial oxidative phosphorylation measured by a new optical method for measuring oxygen concentration. *J. Biol. Chem.* 263:2712–2718.
37. Jones, D. P., and H. S. Mason. 1978. Gradients of O_2 concentration in hepatocytes. *J. Biol. Chem.* 253:4874–4880.
38. Wilson, D. F., M. Erecinska, C. Drown, and I. A. Silver. 1979. The oxygen dependence of cellular energy metabolism. *Arch. Biochem. Biophys.* 195:485–493.
39. Gnaiger, E., R. Steinlechner-Maran, G. Mendez, T. Eberl, and R. Margreiter. 1995. Control of mitochondrial and cellular respiration by oxygen. *J. Bioenerg. Biomembr.* 27:583–596.
40. Marcinek, D. J., W. A. Ciesielski, K. E. Conley, and K. A. Schenkman. 2003. Oxygen regulation and limitation to cellular respiration in mouse skeletal muscle *in vivo*. *Am. J. Physiol. Heart Circ. Physiol.* 285: H1900–H1908.
41. Schumacker, P. T., N. Chandel, and A. G. Agusti. 1993. Oxygen conformance of cellular respiration in hepatocytes. *Am. J. Physiol.* 265:L395–L402.
42. Subramanian, R. M., N. Chandel, G. R. Budinger, and P. T. Schumacker. 2007. Hypoxic conformance of metabolism in primary rat hepatocytes: a model of hepatic hibernation. *Hepatology.* 45:455–464.